Development 134, 4063-4072 (2007) doi:10.1242/dev.008722

Axonal wiring of guanylate cyclase-D-expressing olfactory neurons is dependent on neuropilin 2 and semaphorin 3F

Andreas Walz, Paul Feinstein, Mona Khan and Peter Mombaerts*

The olfactory system of the mouse includes several subsystems that project axons from the olfactory epithelium to the olfactory bulb. Among these is a subset of neurons that do not express the canonical pathway of olfactory signal transduction, but express guanylate cyclase-D (GC-D). These GC-D-positive (GC-D$^+$) neurons are not known to express odorant receptors. Axons of GC-D$^+$ neurons project to the necklace glomeruli, which reside between the main and accessory olfactory bulbs. To label the subset of necklace glomeruli that receive axonal input from GC-D$^+$ neurons, we generated two strains of mice with targeted mutations in the GC-D gene (*Gucy2d*). These mice co-express GC-D with an axonal marker, tau-β-galactosidase or tauGFP, by virtue of a bicistronic strategy that leaves the coding region of the *Gucy2d* gene intact. With these strains, the patterns of axonal projections of GC-D$^+$ neurons to necklace glomeruli can be visualized in whole mounts. We show that deficiency of one of the neuropilin 2 ligands of the class III semaphorin family, Sema3f, but not Sema3b, phenocopies the loss of neuropilin 2 (Nrp2) for axonal wiring of GC-D$^+$ neurons. Some glomeruli homogeneously innervated by axons of GC-D$^+$ neurons form ectopically within the glomerular layer, across wide areas of the main olfactory bulb. Similarly, axonal wiring of some vomeronasal sensory neurons is perturbed by a deficiency of Nrp2 or Sema3f, but not Sema3b or Sema3c. Our findings provide genetic evidence for a Nrp2-Sema3f interaction as a determinant of the wiring of axons of GC-D$^+$ neurons into the unusual configuration of necklace glomeruli.

KEY WORDS: Guanylate cyclase, Semaphorin, Neuropilin, Olfactory bulb, VNO, Necklace glomeruli

INTRODUCTION

The main and accessory olfactory systems of the mouse detect a large variety of chemical stimuli from the external environment. Chemoreception is mediated by several types of receptor molecules that are expressed by specialized sensory neurons (Axel, 2005; Buck, 2005; Mombaerts, 2004). The information gathered by the sensory neurons in the periphery is relayed to the brain through anatomical structures called glomeruli, which reside in the main and accessory olfactory bulbs.

In the past decade, many studies have concentrated on the elucidation of the mechanisms of sensory neuron differentiation and axonal wiring in the mouse. Most of the efforts have been on the two major cell types of the olfactory system, olfactory sensory neurons (OSNs), expressing odorant receptor (OR) genes, and vomeronasal sensory neurons (VSNs), expressing vomeronasal receptor (VR) genes. Axons of OSNs expressing the same OR project to a small subset of glomeruli at reproducible positions, and ORs are intimately involved in axonal wiring of OSNs (Mombaerts, 2006).

There are several other olfactory subsystems, which have received much less attention. The first of these is an island of olfactory nature, the septal organ, which is located within the respiratory epithelium on the ventral aspect of the posterior septum (Rodolfo-Masera, 1943). This structure contains neurons that express a subset of ORs shared with OSNs that reside in the ventral regions of the main olfactory epithelium (MOE) and that project their axons to the ventral parts of the main olfactory bulb (MOB). The OR expression profile of the septal organ has similarities and differences with the MOE (Tian and Ma, 2004). The specific function of the septal organ has not been established; its neurons may also have mechanosensory abilities (Grosmaitre et al., 2007). Second, the Grueneberg ganglion, located at the tip of the nose (Grueneberg, 1973), is now regarded as an olfactory subsystem (Fuss et al., 2005; Koos and Fraser, 2005; Fleischer et al., 2006; Roppolo et al., 2006). Its function is not known. Third, a family of G-protein-coupled receptors, the TAARs, is expressed in a subset of sensory neurons of the MOE (Liberles and Buck, 2006). Fourth, several types of neurons in the MOE project their axons to the necklace area, which demarcates the main from the accessory olfactory bulb. Several markers distinguishes these neurons from OR-expressing OSNs or VR-expressing VSNs: placental antigen X-P2 (Shinoda et al., 1989; Shinoda et al., 1993), antigens to antibodies 2C6 and mAb213 (Ring et al., 1997), and guanylate cyclase-D (GC-D) (Fülle et al., 1995; Juilfs et al., 1997). Neurons from the Grueneberg ganglion also project to the necklace area (Fuss et al., 2005). Thus, the necklace area is heterogeneous in axonal input. Little is known about the function, morphology and development of the necklace area, or about the various types of cells that project their axons to it.

We have demonstrated a major role for neuropilin 2 (Nrp2) in VSN axonal wiring and glomerular formation in the accessory olfactory bulb (AOB), and a minor role in OSN axonal projections to the MOB (Walz et al., 2002). The necklace area is also disorganized in our *Nrp2* mutant mice. Several of these phenotypes were observed in another strain of *Nrp2* mutant mice (Cloutier et al., 2002). Neuropilins are co-receptors for class III semaphorins, and Nrp2 binds Sema3b, Sema3c and Sema3f (Chen et al., 1997; Kolodkin et al., 1997; Takahashi et al., 1998).

Here, we assess the contributions of individual semaphorin ligands to the phenotypes that are observed in the necklace area of *Nrp2* mutant mice. We labeled a subset of necklace glomeruli by generating two mouse strains with targeted mutations in the GC-D (*Gucy2d*) locus that produce bicistronic messages resulting in co-translation of GC-D with an axonal marker, tau-β-galactosidase or tauGFP (tau is also known as Mapt). A striking phenotype of *Nrp2*

The Rockefeller University, 1230 York Avenue, New York, NY 10021, USA.

*Author for correspondence (e-mail: peter@rockefeller.edu)

Accepted 28 August 2007

or *Sema3f* knockout mice is that axons of GC-D-positive (GC-D$^+$) neurons, which are not known to express ORs, coalesce into homogeneous glomeruli that are scattered widely at ectopic locations within the glomerular layer of the MOB, in addition to glomeruli in normal positions. Our findings provide genetic evidence for a Nrp2-Sema3f interaction as a determinant of axonal wiring of GC-D$^+$ neurons, and also for axons of some VSNs.

MATERIALS AND METHODS

Targeting of the *Gucy2d* locus

A probe corresponding to the last exon of the ORF of the rat GC-D gene was used to screen a 129/SvJ mouse BAC library (Genome Systems, St Louis, MO, USA). From the resulting BAC clone 112J14, a *Hin*dIII fragment containing the 3′ end of the *Gucy2d* gene was subcloned into pBS-SKII (Stratagene, La Jolla, CA, USA). To shorten its length for the right arm, a re-ligation between the *Xho*I site within pBS-SKII at the 3′ end of the subcloned *Hin*dIII fragment and an internal *Xho*I was performed. Next, an *Eco*RI fragment was inserted at the 5′ end to lengthen the left arm, to create a targeting vector with a 2.8 kb left arm and 6 kb right arm. A *Pac*I site was generated 3 bp after the stop codon in exon 19 of the ORF by PCR mutagenesis and placed into the targeting vector by *Nco*I-*Sac*I subcloning. A *Pme*I site was generated at the 5′ end of the targeting vector for linearization. A cassette consisting of *IRES-tauGFP* or *IRES-taulacZ*, and a self-excising *pgk-neomycin* expression cassette flanked by *loxP* sites (ACNF) (Bozza et al., 2002) was placed into the newly generated *Pac*I site. The green fluorescent protein (GFP) version was EGFP-1 (Clontech, Palo Alto, CA).

Targeting of the *Sema3b* and *Sema3f* loci

To construct targeting vectors, the left and right arms were amplified using the GeneAmp XL PCR kit (Applied Biosystems, Alameda, CA) with genomic DNA of E14 cells as template. The following oligos were used: *Sema3b* right arm forward: GCGCGTTAATTAAGGACCACGTAGTGCAGCTCACTGGTGA, reverse: ATATAGGCGCGCCTAGAGCCCAGCAGTACAACATGGCCACC; *Sema3b* left arm forward: GGCCGTTTAAACGCCTTACCACCCCCTGGCACTAAGCTC, reverse: TATAAGCGGCCGCTAAAGGAGAGCCGAAGGCGGGGAAGGTT; *Sema3f* right arm forward: GCGCGCTTAATTAACAGTGATCGGCGCCGTGAGGTGAGTT, reverse: ATATAGGCGCGCCAGGGGCTGGAGAGATGGTCAGTGG; *Sema3f* left arm forward: GGCCGTTTAAACGGCAGTGGTTCTCAACCTTCTTAGCTGCCAC, reverse: TATAAGCGGCCGCGGTACCGGTGGCCTTAAGTTCTGTGG. The arms, which were between 3.8 kb and 4.4 kb, were subcloned into a modified pBS-SKII vector and sequenced for PCR errors. A *Pme*I site was generated at the 5′ end of the targeting vector for linearization of the construct. ACNF was placed in an *Xba*I site between the left and right arms.

Gene targeting

Genomic DNA from G418-resistant ES colonies of E14 was digested with *Bam*HI for *Gucy2d*, *Hin*dIII for *Sema3b* and *Bam*HI for *Sema3f* and analyzed by Southern blot hybridization with a 5′ external probe for *Gucy2d*, and 3′ external probes for *Sema3b* and *Sema3f*. DNA of positive clones was digested with *Hin*dIII or *Eco*RI for *Sema3b* and *Sema3f*, respectively, and probed with 5′ external probes to verify that no large-scale genomic reorganizations had occurred. ES cells were injected into C57BL/6J blastocysts. Mice were in a mixed 129 × C57BL/6J background. The strains will be available from The Jackson Laboratory, as follows: strain name B6;129P2-*Gucy2d*^{tm1Mom}/MomJ and #6703 for GCD-ITL; strain name B6;129P2-*Gucy2d*^{tm2Mom}/MomJ and #6704 for GCD-ITG; strain name B6;129P2-*Sema3b*^{tm1Mom}/MomJ and #6705 for ΔB; strain name B6;129P2-*Sema3f*^{tm1Mom}/MomJ and #6710 for ΔF. The GCD-ITG mice have been described, in part, previously (Hu et al., 2007).

The *Sema3c* gene has previously been mutated by us (Feiner et al., 2001). We have here studied the *Sema3c*$^{tm1.1Jra}$ strain in a genetic background that allows for postnatal survival.

Experiments were conducted according to guidelines and with approval from the Institutional Animal Care and Use Committee of The Rockefeller University.

Fluorescent immunohistochemistry, β-galactosidase and GFP visualization

For immunohistochemistry, mice were deeply anaesthetized and intracardially perfused with 4% paraformaldehyde (pH 7.4), postfixed on ice for 3 hours and finally sunk in 30% sucrose overnight. They were then frozen in OCT and 16-18 μm sections were cut on a cryostat. Sections were blocked in 10% normal donkey serum (NDS) for 1 hour at room temperature followed by incubation with primary antibodies in blocking solution at 4°C overnight, except for MAP2 stainings which were incubated for 2 days. The following day the sections were washed in 0.1% Triton X-100 in PBS and incubated with secondary antibody for 1 hour at room temperature. After final washes in 0.1% Triton X-100 in PBS, sections were stored in PBS until viewed. Primary antibodies used are as follows: rabbit polyclonal anti-PDE2A at 1:100 (FabGennix, Frisco, TX, USA), rabbit polyclonal anti-β-galactosidase at 1:500 (MP Cappel, Solon, OH, USA) and chicken polyclonal anti-β-galactosidase at 1:500 (Abcam, Cambridge, MA, USA), donkey polyclonal anti-OMP at 1:5000 (Wako Chemicals USA, Richmond, VA, USA), and rabbit polyclonal anti-MAP2 at 1:1000 (Abcam). Secondary antibodies were: Alexa Fluor 488-conjugated donkey anti-rabbit, Alexa Fluor 546-conjugated donkey anti-rabbit, donkey anti-goat and donkey anti-chicken (Invitrogen, Carlsbad, CA, USA), and Cy5 donkey anti-rabbit (Jackson ImmunoResearch Laboratories, West Grove, PA, USA) all at 1:500.

For β-galactosidase whole-mount analysis, tissues were processed as described before (Mombaerts et al., 1996), except that the fixation was carried out on ice for 5 minutes. X-Gal-stained whole-mount specimens were examined with a Zeiss SV11 stereomicroscope, and images were taken with a Zeiss AxioCam CCD camera. For *tauGFP/taulacZ* whole-mounts, mice were sacrificed by CO_2 asphyxiation and the olfactory epithelium exposed. Staining procedures were performed as described before (Feinstein and Mombaerts, 2004). Whole-mounts of *tauGFP*, GFP sections and immunostained sections were examined with a Zeiss LSM 510 confocal microscope. Image files were processed with Adobe Photoshop 8.0.

Glomerular measurements

Measurements of GC-D$^+$ glomeruli were performed on whole-mount bulbs of GCD-ITL homozygous mice that were lightly stained (<1 hour exposure to X-Gal at room temperature). The short staining period was necessary to avoid staining in axons that could obscure smaller glomeruli. Counting of glomeruli was performed with a Zeiss SV11 stereomicroscope, and size measurements were done on images taken with a Zeiss AxioCam CCD camera. The longest axis of individual glomeruli were measured with Adobe Photoshop 8.0 and Canvas 6.0. Student's *t*-tests were used to determine the significance of changes between glomerular counts and sizes.

RESULTS

Targeted mutagenesis of the *Gucy2d* gene

To label specifically the subset of necklace glomeruli that receive axonal input from GC-D$^+$ neurons (Fülle et al., 1995; Juilfs et al., 1997), we engineered two strains of mice to co-express GC-D with an axonal marker, tau-β-galactosidase or tauGFP. The *Gucy2d* gene is located on chromosome 7E1 (Yang et al., 1996), spans ~35 kb, and contains at least 22 exons in its open reading frame (ORF) and 5′ untranslated region (Fig. 1A). By homologous recombination in embryonic stem (ES) cells, we created targeted mutations in the *Gucy2d* locus that leave the coding region intact and produce bicistronic messages (Fig. 1B). The mouse strains are referred to as GCD-ITL and GCD-ITG.

In GCD-ITL mice, cell bodies that express β-galactosidase activity, and therefore can be stained blue with X-Gal, reside in a punctate pattern within the MOE, at a higher density towards the ventral aspects of the MOE (Fig. 2A) (Fülle et al., 1995). X-Gal$^+$ cells are also present in the septum, including the septal organ (Fig. 2B), in which a small number of neurons are known to express GC-D (Ma et al., 2003). As described previously for GC-D$^+$ neurons (Juilfs et al., 1997), most X-Gal$^+$ cells reside within the recesses of the ectoturbinates as opposed to the endoturbinates.

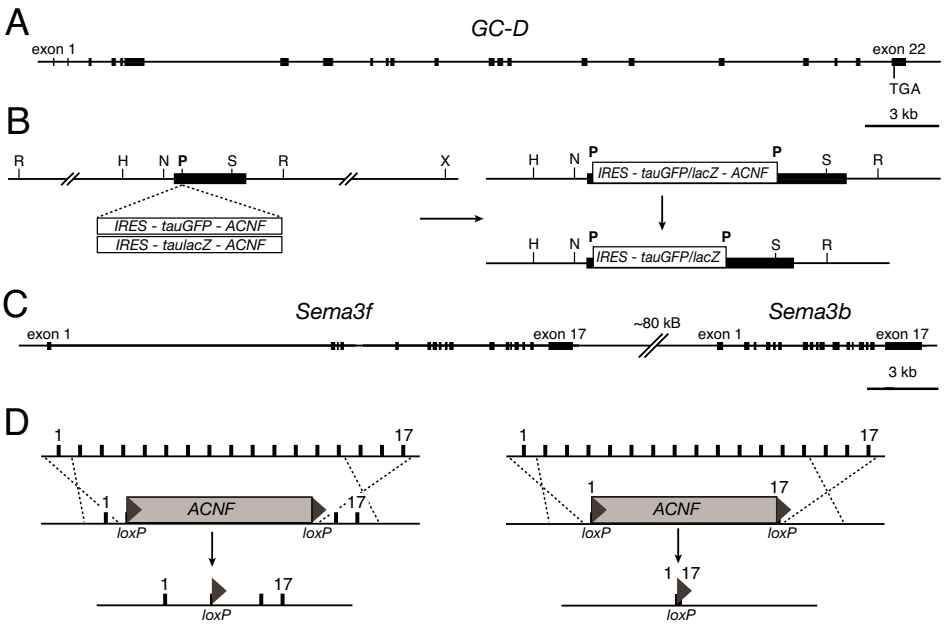

Fig. 1. Targeted mutagenesis of the *Gucy2d, Sema3f* and *Sema3b* loci. (**A**) Genomic structure of the *Gucy2d* locus on chromosome 7E1 according to the NCBI database. The coding region is spread over 19 exons, with at least another three exons at the 5′ untranslated region. No other genes are predicted within the *Gucy2d* locus. (**B**) GC-D knock-in mutations. A *Pac*I site (P) was created 3 bp downstream of the stop codon in exon 22 by PCR subcloning between *Nco*I (N) and *Sac*I (S). The targeting vector encompasses the region from an upstream *Eco*RI (R) site to a downstream *Xho*I (X) site. Left, targeting vector. Right upper, targeted mutation in ES cells. Right lower, targeted mutation after germline transmission. Diagram is not to scale. (**C**) Genomic organization of the *Sema3f* and *Sema3b* loci on chromosome 9F2. The coding regions comprise 17 exons spanning ~22 kb and ~6 kb, respectively. At least three other genes (*Gnai2*, *Slc38a3* and *Gnat1*) are predicted within the 80 kb between *Sema3f* and *Sema3b*. (**D**) Targeting strategies to create knockout mutations of *Sema3f* (left) and *Sema3b* (right). Gene targeting replaces exons 2–15 (*Sema3f*) or exons 1–17 (*Sema3b*) with the ACNF cassette. During germline transmission in male chimeras, the ACNF cassette excises itself, removing most (*Sema3f*) or all (*Sema3b*) of the ORF. Diagrams are not to scale.

GC-D$^+$ cells display the typical morphology of neurons (Fig. 2C,D) with the exception of somewhat shorter cilia. All GFP$^+$ axons in GCD-ITG mice are immunoreactive for PDE2A (Fig. 6A), consistent with the expression of PDE2A by GC-D$^+$ cells in the MOE (Juilfs et al., 1997). In mice that are doubly heterozygous for GCD-ITL and GCD-ITG, GC-D$^+$ neurons co-express β-galactosidase and GFP, demonstrating bi-allelic expression at the *Gucy2d* locus (Fig. 2E).

GC-D$^+$ cell bodies appear before birth, reach peak numbers within the first postnatal week, and decline in the following weeks to reach minimal counts during adulthood (data not shown). Conceivably this decline in labeled cell bodies – which is not seen in labeled axons – is due to transport of tauGFP or tau-β-galactosidase along the ever longer axons, thus depleting the cell bodies of marker protein. We have reported a similar age-related phenomenon for the axons of mitral and tufted cells (Walz et al., 2006).

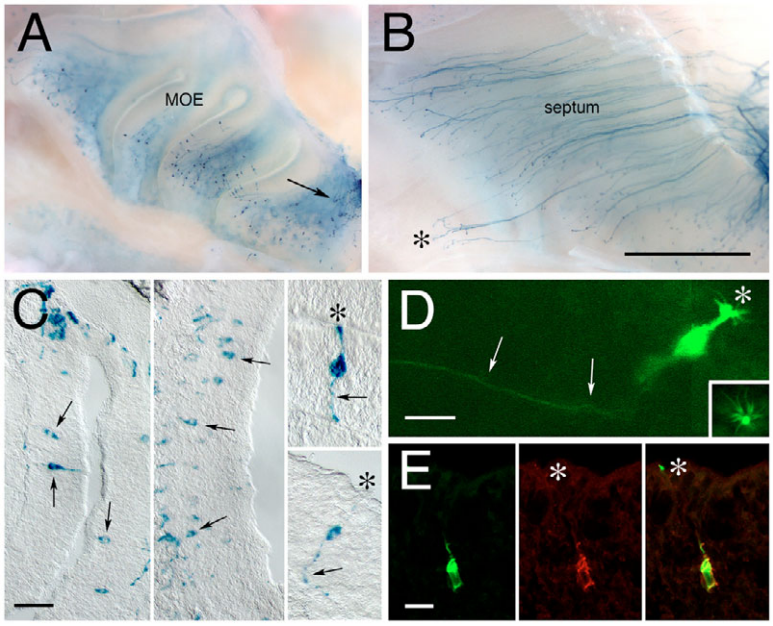

Fig. 2. Characterization of GC-D$^+$ neurons in the MOE. (**A**) Whole-mount view of the turbinates of a GCD-ITL homozygous 3-week-old (3 wk) mouse after X-Gal staining. Labeled cell bodies can be seen on all turbinates, with a greater number situated towards the ventral aspects. The greatest accumulation is located at the caudal end of the MOE (arrow). Anterior. left, dorsal up. (**B**) Whole-mount view of the septal area of a GCD-ITL homozygous mouse (3 wk). A similar distribution pattern as in the turbinates is apparent. Labeled axons take a straight route towards the cribriform plate. A few labeled cells reside within the septal organ (asterisk). (**C**) Sections through the MOE of a GCL-ITL homozygous mouse (P10). Labeled cell bodies (arrows in left and middle panels) reside within the lower layers of the epithelium. The morphology of labeled cells is similar to that of conventional OSNs. Cells extend dendrites towards the lumen (asterisks in right panels) and axons towards the lamina propria (arrows in right panels). (**D**) High-magnification view of a GFP$^+$ cell in a whole-mount of the MOE of a GCD-ITG homozygous mouse (3 wk). A typical neuronal morphology is apparent with a dendrite and dendritic knob (asterisk) and a long axon (arrows). Insert shows en face view of a dendritic knob with GFP$^+$ cilia. (**E**) Sections through the MOE of a GCL-ITG/GCL-ITL double heterozygous mouse (P7). The cell body is positive for the intrinsic fluorescence of GFP (left panel) and β-galactosidase immunofluorescence (middle panel). The combined image is shown on the right. Asterisk in middle and right panels denotes the dendritic knob. Scale bars: 1000 μm A,B; 40 μm C, left two panels; 20 μm C, right panel; 20 μm in D,E.

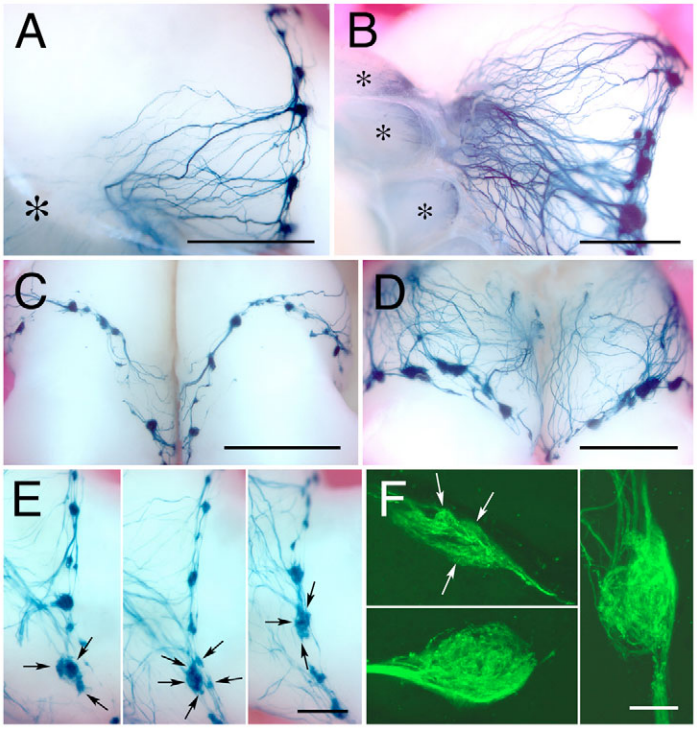

Fig. 3. GC-D$^+$ glomeruli in the necklace area of the olfactory bulb. (**A**) Whole-mount view of the medial OB in an adult GCD-ITL homozygous mouse, stained with X-Gal. Axons enter the bulb through the cribriform plate (asterisk) on the ventral side, and project towards the caudal end of the OB where they form interconnected glomeruli. Anterior, left, dorsal up. (**B**) The lateral OB. A greater number of axons are entering on the lateral side, and larger glomeruli are formed. Asterisks denote the MOE turbinates. (**C**,**D**) The dorsal (C) and ventral (D) OB. Glomeruli are arranged as a closed necklace of beads on a string. Axons projecting from the MOE, glomeruli, and axonal connections between glomeruli are visible ventrally, whereas only glomeruli and axonal connections are visible dorsally. Anterior is up. (**E**) Three examples of lightly X-Gal stained glomeruli on the lateral OB of GCD-ITL homozygous 6-week-old (6 wk) mice. No obvious pattern of glomerular positions is apparent. Larger glomeruli tend to form on the ventral aspects of the bulb. Some glomeruli form a cluster, at a consistent position (arrows). Anterior, left; dorsal, up. (**F**) Section of necklace area in adult GCD-ITG homozygous mice. There are superficially located GFP$^+$ glomeruli in the dorsal aspect (upper left), ventral aspect (lower left) and lateral aspect (right). A cluster of glomeruli can be seen (arrows). Dorsal is up. Scale bars: 1000 μm in A-D; 500 μm in E; 50 μm in F.

Morphology and development of GC-D$^+$ glomeruli

Axons of GC-D$^+$ neurons course through the lamina propria along with OSN axons, penetrate the skull through the cribriform plate, and turn towards the caudal aspect of the MOB along a ventral trajectory (Fig. 3A-D). GC-D$^+$ axons spread out to form several glomeruli, which are located superficially. Often, clustering occurs in arrangements of several tightly packed glomeruli (Fig. 3E,F). GC-D$^+$ glomeruli form a complete ring around the stalk of the MOB and around the anterior part of the AOB (Fig. 3A-D), thus placing them in the necklace area. GC-D$^+$ axons interconnect these glomeruli to form the typical necklace appearance of beads on a string. None of the GC-D$^+$ glomeruli could be identified unequivocally as belonging to the modified glomerular complex, a structure that is poorly defined. Overall, no stereotyped pattern in the positions of GC-D$^+$ glomeruli was apparent among bulbs (Fig. 3E) except that a greater number and the larger glomeruli are located in the ventrolateral aspects of the caudal MOB (Fig. 3B). One exception is the conserved location of a glomerular cluster at the ventral-most position on the lateral side of the MOB (Fig. 3E).

GC-D$^+$ glomeruli are not detectable on postnatal day 1 (P1), although GC-D$^+$ axons are present in the MOB (data not shown). GC-D$^+$ glomeruli form within the first postnatal week. Glomeruli in adults can be divided roughly into three size classes, as measured along the longest surface dimension: small (40-90 μm), medium (100-160 μm) and large (180-300 μm) (Fig. 4A). The number of GC-D$^+$ glomeruli of each size class increases during the first postnatal weeks to reach a maximum at 6 weeks (6 wk), and remains constant at 12 wk (Fig. 4B).

Targeted mutagenesis of the *Sema3b* and *Sema3f* genes

What are the mechanisms that underlie the wiring of axons of GC-D$^+$ neurons into this unusual arrangement of necklace glomeruli? We have reported that a mutation in the neuropilin 2 gene (strain NP2-Δ) perturbs the projection of some VSN axons to the AOB, and also produces a general disorganization of the necklace area (Walz et al., 2002). Most GC-D$^+$ neurons express neuropilin 2 (Nrp2; Fig. 6B). Nrp2 has been proposed as a co-receptor for several class III semaphorins, most notably Sema3b, Sema3c and Sema3f (Chen et al., 1997; Kolodkin et al., 1997; Takahashi et al., 1998). To investigate the individual contributions of semaphorins in the wiring defects of GC-D$^+$ axons seen in *Nrp2* mutant mice, we generated *Sema3b* and *Sema3f* knockout mice by gene targeting.

The *Sema3f* and *Sema3b* genes are located on chromosome 9F2 within 80 kb of each other (Fig. 1C). We created individual null mutations for both *Sema3f* (henceforth called ΔF) and *Sema3b* (henceforth called ΔB) by deleting 85% (ΔF) or 100% (ΔB) of the ORF (Fig. 1D). Compared with other targeted mutations of *Sema3f* (Sahay et al., 2003) and *Sema3b* (Julien et al., 2005), ΔF and ΔB are null mutations.

The ΔF and ΔB mouse strains are viable as homozygotes. ΔF homozygous mice display many of the gross defects we observed in NP2-Δ homozygous mice (Walz et al., 2002), including reduced size of the mice during the first few weeks after birth and a smaller number of homozygous mice than expected from a Mendelian distribution (n=34 for wild type, n=51 for heterozygous, n=14 for homozygous). ΔB homozygous mice appear normal and are born at Mendelian frequencies (n=28 for wild type, n=47 for heterozygous, n=21 for homozygous). ΔB/ΔF double mutants could not be generated because of the linkage of these genes in the genome.

Axonal wiring of GC-D$^+$ neurons in Nrp2- and Sema3f-deficient backgrounds

To evaluate a role for neuropilin-semaphorin signaling in axonal wiring of GC-D$^+$ neurons, GCD-ITL mice were crossed with NP2-Δ, ΔB, and ΔF mice. GC-D$^+$ axons fan out over a far greater territory of the MOB in a NP2-Δ homozygous background than in wild-type mice, and glomeruli form in inappropriate locations (Fig. 5). In addition to GC-D$^+$ glomeruli that are located in the necklace area, many GC-D$^+$ glomeruli are scattered ectopically across the

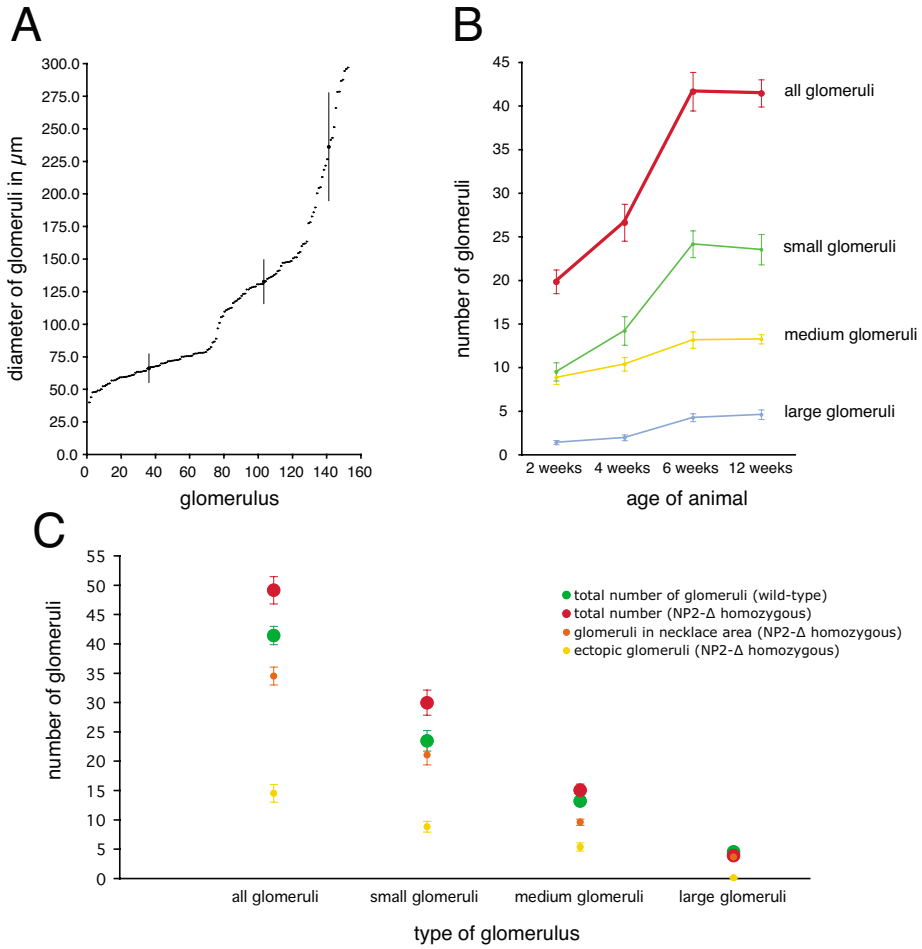

Fig. 4. Numbers of GC-D$^+$ glomeruli. (**A**) Graph of glomerular size in adult GCD-ITL mice (n=8 bulbs). The longest diameter of a given GC-D$^+$ glomerulus was measured. Three classes of glomeruli can be distinguished: large, 236.2±41.4 μm (n=24); medium, 132.9±20.2 μm (n=53); small, 66.6±10.9 μm (n=75). (**B**) Graph of developmental series of the number of GC-D$^+$ glomeruli per bulb, at 2 weeks postnatal (2 wk; n=9 bulbs), 4 wk (n=12), 6 wk (n=10) and 12 wk (n=14). (**C**) Graph of numbers of glomeruli in NP2-Δ homozygous, GCD-ITL homozygous mice compared to GCD-ITL homozygous ('wild-type') mice.

MOB up to the rostral tip. There are fewer GC-D$^+$ glomeruli in the necklace area compared to controls, but the combined number of necklace and ectopic GC-D$^+$ glomeruli in the NP2-Δ homozygous background is significantly greater compared to wild-type mice (Fig. 4C). Large glomeruli form almost exclusively in the necklace area and are equally frequent in mutant and wild-type mice. Similar numbers of medium-sized glomeruli are found in mutant and wild-type mice, but some glomeruli are ectopic in mutant mice. Significantly more small glomeruli form ectopically in mutant mice, accounting for most of the increase of total number of glomeruli in mutant mice.

The defects in the NP2-Δ homozygous background are phenocopied in the ΔF homozygous background (Fig. 5). By contrast, ΔB homozygous mice (Fig. 5) and *Sema3c* homozygous mutant mice (data not shown) have a normal GC-D innervation pattern among the necklace glomeruli.

To further investigate the composition of ectopic GC-D$^+$ glomeruli in NP2-Δ homozygous mice, we tested whether the ectopic glomeruli receive axonal input solely from GC-D$^+$ neurons, or whether they may have heterogeneous innervation by neurons from the MOE. By double labeling ectopic GC-D$^+$ glomeruli in the MOB with antibodies against OMP, no GC-D$^-$/OMP$^+$ areas were detected within these glomeruli, indicating that axons of other types of OMP$^+$ neurons do not contribute to these glomeruli, at least not in substantial numbers (Fig. 6C). Ectopic GC-D$^+$ glomeruli were found to reside at appropriate, deeper, locations within the glomerular layer of the MOB, instead of at the superficial locations in the necklace area (Fig. 6A,C). Furthermore, when ectopic GC-D$^+$ glomeruli were counterstained with antibodies against MAP-2 to visualize mitral and tufted cell dendrites projecting to glomeruli, these glomeruli were doubly labeled (Fig. 6D). Thus, the homogeneous innervation of ectopic glomeruli by axons of GC-D$^+$ neurons and the projections of dendrites of mitral and tufted cells into these ectopic glomeruli, suggest that these glomeruli may represent new functional units.

Axonal wiring of VSNs in Nrp2- and Sema-deficient backgrounds

The NP2-ΔΔ mutation also perturbs the projection of VSN axons to the AOB (Walz et al., 2002). To evaluate a role of Sema3b, Sema3c and Sema3f in axonal wiring of VSNs, the targeted mutations in the corresponding genes were introduced into NP2-Δ (Walz et al., 2002) heterozygous, or V1rb2-IRES-taulacZ (Rodriguez et al., 1999) homozygous backgrounds to visualize, respectively, the Nrpn2$^+$ axonal population emanating from apical VSNs (expressing the entire repertoire of *V1r* genes), and the axonal population of V1rb2$^+$ VSNs (expressing the *V1r* gene *V1rb2*). The NP2-Δ mutation is used in the heterozygous state merely as a marker for apical VSNs, and in the homozygous state both as a marker for apical VSNs and to assess the consequences of loss of Nrp2.

In the ΔF homozygous background, the cell bodies of Nrp2$^+$ VSNs were still located within the apical layer of the VNO, and the numbers and distribution of V1rb2$^+$ VSNs were normal (data not

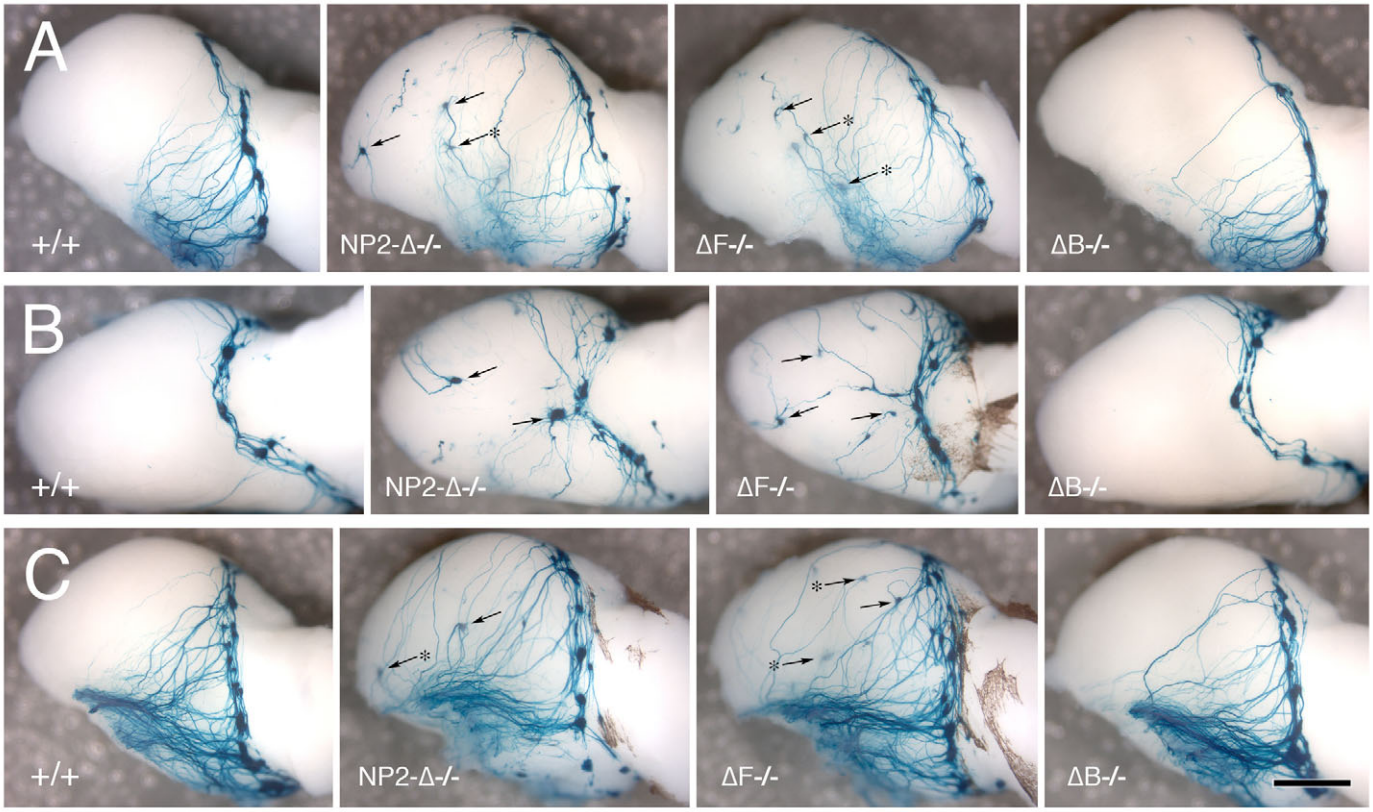

Fig. 5. Axonal wiring of GC-D$^+$ neurons depends on Npr2 and Sema3f. (**A**) Whole-mount view of the medial OB of GCD-ITL homozygous mice visualized by X-Gal staining in wild-type (+/+), NP2-Δ homozygous (NP2-Δ –/–), ΔF homozygous (ΔF –/–), and ΔB homozygous (ΔB –/–) backgrounds. The innervation pattern in ΔB homozygous mice is similar to that in wild type. NP2-Δ and ΔF homozygous mice have axons that extend not only in the ventral areas, but also in the dorsal and anterior aspects of the MOB where they form ectopic glomeruli (arrows). Several of these glomeruli form in the deeper layers of the MOB (arrows with asterisks). Anterior, left; dorsal up. (**B**) Whole-mount view of the dorsal OB of GCD-ITL homozygous mice in the same backgrounds as in A. Labeled axons and glomeruli (arrows) are detectable in NP2-Δ and ΔF homozygous mice in areas that are not occupied in wild-type and ΔB homozygous mice. Anterior left, lateral up. (**C**) Whole-mount view of the lateral OB of GCD-ITL homozygous mice in the same backgrounds as in A and B. As seen medially, ectopic glomeruli (arrows) are observed that reside sometimes in deeper layers (arrows with asterisks). Anterior left, dorsal up. Scale bar: 1000 μm.

shown). However, the axonal projections of Nrp2$^+$ and V1rb2$^+$ VSNs exhibited defasciculation across the medial surface of the MOB (Fig. 7D), as we reported for NP2-Δ homozygous mice (Fig. 7C) (Walz et al., 2002). By contrast, axonal projection patterns appeared normal in ΔB and *Sema3c* homozygous mutant backgrounds (Fig. 7A,B, and data not shown).

No miswiring of V1rb2$^+$ axons into the MOB was observed in whole-mount preparations of ΔF homozygous mice (Fig. 7D) or in sections (data not shown). Most Nrp2$^+$ axons and all V1rb2$^+$ axons eventually reached the AOB (Fig. 7C,D). Within the anterior AOB (aAOB), Nrp2$^+$ axons erroneously project into the posterior AOB (pAOB) in a ΔF homozygous background (Fig. 7H), comparable to the phenotype of NP2-Δ homozygous mice (Fig. 7G). Likewise, V1rb2$^+$ axons form glomeruli within the pAOB in a ΔF homozygous background (Fig. 7I-L). Interestingly, misprojections can be observed in some mice with a ΔF heterozygous background (18.2%, n=11; Fig. 7L). By contrast, ΔB homozygous and *Sema3c* homozygous mutant mice do not show abnormal innervation patterns for Nrp2$^+$ and V1rb2$^+$ axons into the pAOB (Fig. 7A,F, and data not shown). Axonal overshooting of OSNs observed for NP2-Δ homozygous mice (Walz et al., 2002) occurs in ΔF homozygous mice, but not in ΔB or *Sema3c* homozygous mutant mice (data not shown).

Thus, as for GC-D$^+$ neurons, the defects in VSN axonal wiring caused by a deficiency in Nrp2 can be phenocopied by loss of one of its ligands, Sema3f, but not of Sema3b or Sema3c.

DISCUSSION

This study provides genetic evidence for a functional interaction between Nrp2 and Sema3f in axonal wiring of GC-D$^+$ neurons that produces the unusual arrangement of necklace glomeruli: knockout mice for either *Nrp2* or *Sema3f* have very similar phenotypes. We have hereby extended our approach of targeted integration of axonal marker genes to GC-D$^+$ neurons, which project their axons to the necklace glomeruli, an area of the olfactory bulb that is poorly characterized. In *Nrp2* or *Sema3f* knockout mice, some axons of GC-D$^+$ neurons, which are not known to express ORs, coalesce into glomeruli ectopically within the glomerular layer across the MOB. Some VSN axons are also dependent on Nrp2 and Sema3f for their wiring.

Necklace glomeruli

Much of the focus of research on the olfactory system of the mouse has been on OSNs and VSNs. There has been relatively little progress in our knowledge of other subsystems such as the necklace area, a ring of interconnected glomeruli that surrounds the caudal

end of the MOB and the aAOB in mouse and rat (Juilfs et al., 1997; Ring et al., 1997; Shinoda et al., 1989; Shinoda et al., 1993; Walz et al., 2002; Zheng et al., 1987). Several markers can be used to distinguish the necklace glomeruli from MOB glomeruli, including the high intensity cholinesterase glomeruli also known as atypical glomeruli (Le Jeune and Jourdan, 1993; Zheng et al., 1987), the placental antigen X-P2 immunoreactive glomeruli (Shinoda et al., 1989; Shinoda et al., 1993), the 2C6 and mAb213-positive glomeruli (Ring et al., 1997) and GC-D and PDE2-expressing glomeruli (Fülle et al., 1995; Juilfs et al., 1997). Glomeruli can be positive for one or more of these markers, as well as for the presence or absence of NCAM or OMP (Ring et al., 1997), thus defining multiple classes. They aggregate into 9-16 larger glomerular complexes of differently labeled glomeruli (Ring et al., 1997; Shinoda et al., 1993). The Grueneberg ganglion projects to the necklace area (Fuss et al., 2005), adding to the heterogeneity.

In our GC-D-tagged mouse strains, the number of GC-D$^+$ glomeruli (~40 per bulb) was higher than other types such as mAb213- and 2C6-positive glomeruli [~20 per bulb and ~3 per rat bulb, respectively (Ring et al., 1997)], atypical glomeruli [~15-20 per mouse bulb (Weruaga et al., 2001)] and X-P2 positive glomeruli [~9 per rat bulb (Shinoda et al., 1989)]. These discrepancies may result from differences in methods to visualize or define glomeruli; it may be easier to miss glomeruli in serial sections compared to whole mounts, which may explain our higher counts. As observed with other markers for necklace glomeruli (Le Jeune and Jourdan, 1991; Shinoda et al., 1993), GC-D$^+$ glomeruli only appear well after birth and are not fully formed until 6 weeks, at the onset of sexual maturity.

Signaling in GC-D expressing neurons

GC-D belongs to a class of receptor GCs that contains at least seven members, GC-A to GC-G (Kuhn, 2003). All neurons in the MOE express some membrane GCs (Moon et al., 1998), but GC-D is unique to a small subset of neurons. GC-D$^+$ neurons lack components of the signal transducing mechanism found in conventional OSNs, such as G_{olf}, high affinity cAMP-specific phosphodiesterase, adenylyl cyclase III and the cyclic nucleotide-gated channel subunit CNGA2 (Juilfs et al., 1997; Meyer et al., 2000). GC-D$^+$ neurons may rely on cGMP as a second messenger (Fülle et al., 1995; Juilfs et al., 1997). It is possible that GC-D$^+$ neurons do not use an OR for detection of chemosensory stimuli; they are not known to express ORs. GC-D itself may function as the primary mechanism for stimulus reception in these neurons; alternatively, another class of chemosensory receptor(s) is expressed in GC-D$^+$ neurons.

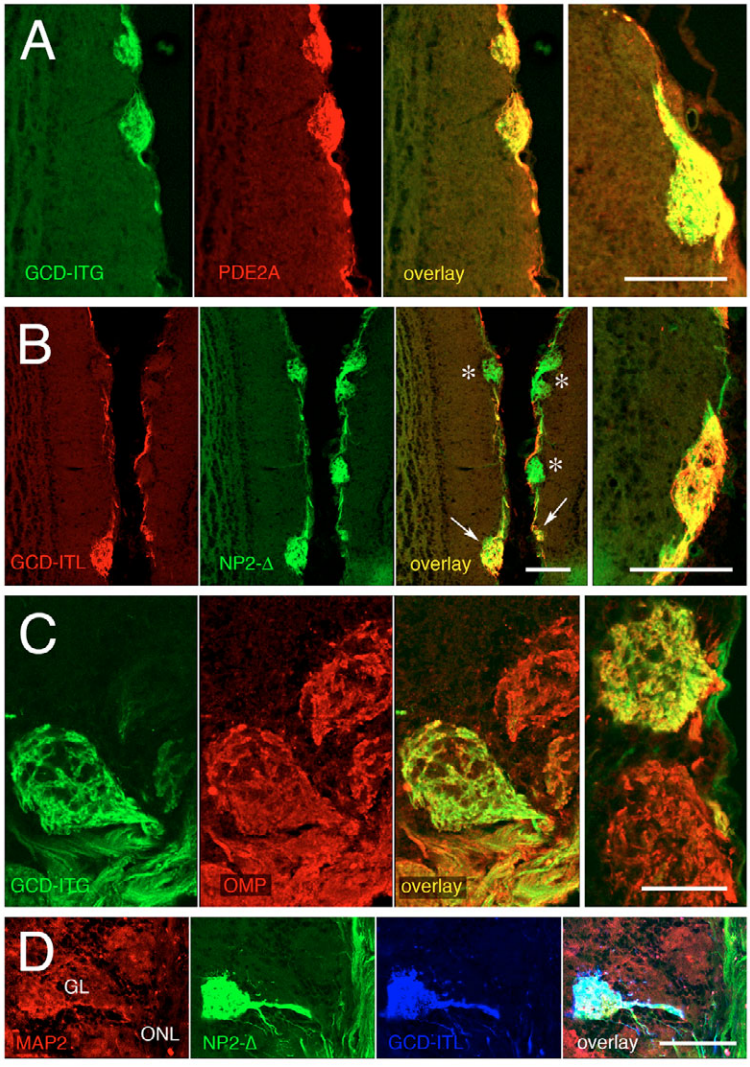

Fig. 6. Immunohistochemistry of necklace and ectopic glomeruli. (**A**) Sections (18 μm) through the caudal OB at the level of the necklace area of a GCD-ITG homozygous mouse stained with an antibody to PDE2A. All GFP$^+$ axons (green) are also PDE2A$^+$ (red), and are thus yellow in the overlay image. Right-most panel: large glomerulus. Dorsal is up. (**B**) Sections (18 μm) through the caudal OB at the level of the necklace area of a GCD-ITL homozygous, NP2-Δ heterozygous mouse stained with an antibody to β-galactosidase (red). A subset of Nrp2$^+$ (GFP; green) glomeruli is also positive for β-galactosidase (arrows); other necklace glomeruli are only Nrp2$^+$ (asterisks). All GC-D$^+$ glomeruli are also Nrp2$^+$ (yellow in overlay). Right-most panel: high magnification. Dorsal is up. (**C**) Sections (18 μm) through the OB of a GCD-ITG homozygous, ΔF homozygous mouse stained with antibodies to OMP (red). Green is the intrinsic green fluorescence of GFP. Three left panels: a high-magnification view of an ectopic glomerulus that is filled by GC-D$^+$ axons (yellow in overlay), at the midlevel of the OB outside the necklace area. Right-most panel: example of glomeruli in the necklace area. A GC-D$^+$ glomerulus (red and green) above a GC-D$^-$ glomerulus (red only). Ectopic glomeruli reside deeper than glomeruli in the necklace area. Dorsal is up. (**D**) Sections (18 μm) through the midlevel OB outside the necklace area of a GCD-ITL homozygous, NP2-Δ homozygous (GFP; green) mouse stained with antibodies to MAP2 (red) and β-galactosidase (blue). MAP2 stained dendrites fill the glomeruli in the glomerular layer (GL) including the ectopic GC-D$^+$/Nrp2$^+$ glomerulus (light blue in overlay image), but are absent in the outer nerve layer (ONL). Scale bars: 100 μm in A,B,D; 50 μm in C.

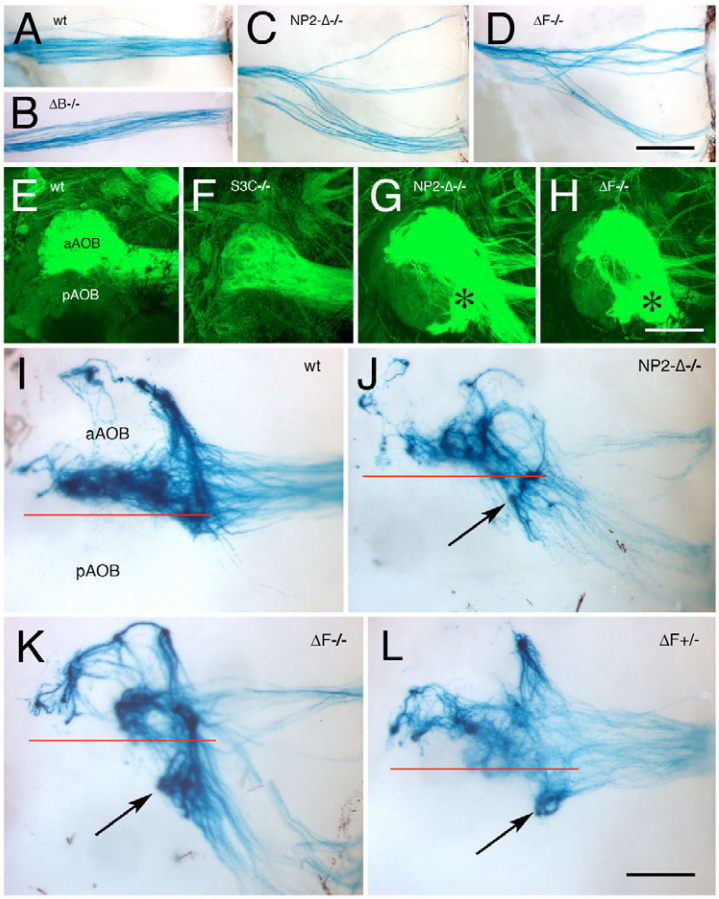

Fig. 7. Aberrant VSN axonal projections in NP2-Δ and ΔF mutant mice. (**A**) Whole-mount view of the medial surface of the MOB. X-Gal staining of adult V1rb2-IRES-taulacZ homozygous mice that are otherwise wild-type (wt). Dorsal is up, anterior left. (**B**) Whole-mount view of the medial surface of the MOB. X-Gal staining of adult V1rb2-IRES-taulacZ homozygous mice that are ΔB homozygous (ΔB–/–). No differences are observed in the axon tracts of V1rb2$^+$ VSNs compared with A. (**C**) Axonal projections of V1rb2$^+$ VSNs across the MOB in a NP2-Δ homozygous, V1rb2-IRES-taulacZ homozygous background. V1rb2$^+$ axons penetrate the cribriform plate (left side) and form tightly packed bundles, but then become much less fasciculated and spread out over a greater area of the MOB. Axons eventually reach and innervate the AOB, which is located at the posterior (right) side of the MOB. (**D**) A pattern similar to that in C is seen for V1rb2$^+$ VSN axons in a ΔF homozygous, V1rb2-IRES-taulacZ homozygous background. (**E-H**) Whole-mount view of the left caudodorsal OB. (E) GFP fluorescence of Nrp2$^+$ VSN axons of a NP2-Δ heterozygous, *Sema3f* wild-type (wt) mouse at 3 weeks postnatal (3 wk). The heterozygous NP-Δ mutation is used as a marker for apical VSNs. Axons innervate only the anterior AOB (aAOB). No Nrp2$^+$ axons occupy the posterior AOB (pAOB). Anterior is top, medial to the right. (F) GFP fluorescence of Nrp2$^+$ axons of a *Sema3c* homozygous mouse at 4 wk. The heterozygous NP2-Δ mutation is used as a marker for apical VSNs. Axon tracts arrive medially to innervate the aAOB. (G) GFP fluorescence of Nrp2$^+$ VSN axons in a NP2-Δ homozygous mouse. VSN axons also cover the medial half of the pAOB (asterisk). (H) GFP fluorescence of Nrp2$^+$ VSN axons in a NP2-Δ heterozygous, ΔF homozygous mouse. The heterozygous NP2-Δ mutation is used as a marker for apical VSNs. Similar to G, there are misprojections to the pAOB (asterisk). (**I-L**) Axonal innervation of the aAOB by V1rb2$^+$ VSNs (V1rb2-IRES-taulacZ homozygous background) as visualized by X-Gal staining of whole mounts. All axons remain anterior in a wild-type adult mouse (I). In a NP2-Δ homozygous mouse, V1rb2$^+$ axons also project to the pAOB (arrow in J). A similar phenotype is seen in a ΔF homozygous background (arrow in K). A less severe misrouting can be seen in some ΔF heterozygous mice, with a few axons veering to the pAOB forming small glomerular structures (arrow in L). Innervation patterns in the anterior AOB are comparable in all backgrounds. The red line demarcates the aAOB from the pAOB. Anterior is top, medial to the right. Scale bars: 500 μm in A-D; 150 μm in E-H; 100 μm in I-L.

We have recently shown that GC-D$^+$ neurons respond specifically to carbon dioxide (Hu et al., 2007), but GC-D itself has not yet been implicated in this response. It is possible that these neurons also respond to other chemicals.

Commonalities between GC-D$^+$ neurons and apical VSNs

GC-D$^+$ necklace glomeruli appear more like glomeruli in the AOB (Belluscio et al., 1999; Rodriguez et al., 1999) than in the MOB, and the necklace area is in the proximity of the AOB. Many of the necklace glomeruli, including GC-D$^+$ glomeruli, develop postnatally, which is consistent with a role for complex behaviors in adult mice. Atypical glomeruli show a sexually dimorphic distribution, further suggesting a function in intraspecies behavior (Weruaga et al., 2001). It is, therefore, unlikely that necklace glomeruli play a role in the suckling behavior as was previously suggested (Shinoda et al., 1993). The modified glomerular complex expressing high intensity cholinesterase, by contrast, appears early on and may still be important for suckling in newborns (Greer et al., 1982), but another study suggested otherwise (Risser and Slotnick, 1987). We could not determine a contribution of GC-D$^+$ glomeruli to the modified glomerular complex, a problem that may be due to the loose definition of this structure.

Mechanisms of axonal wiring defects

The most probable explanation for the miswiring of many GC-D$^+$ axons into ectopic glomeruli across the MOB may lie in the expression of Sema3f over most of the surface of the MOB (Cloutier et al., 2002; Cloutier et al., 2004; Walz et al., 2002). In wild-type mice, Sema3f would deflect the ventrally arriving axons away from dorsal areas such that these axons coalesce into glomeruli in ventral areas; this effect would occur on Nrp2$^+$, OR-expressing OSNs and the Nrp2$^+$ GC-D$^+$ neurons. In the absence of Nrp2 or Sema3f, GC-D$^+$ axons would be free to navigate across ectopic areas of the MOB, and conventional OSNs show an overshooting phenotype (Walz et al., 2002). It cannot be ruled out that Sema3f induces Nrp2$^+$ axons to undergo specific differential adhesion. It is more likely that Sema3f exerts its function as a repellent, causing Nrp2$^+$ growth cones to steer towards areas with lowest possible Sema3f concentration via a localized collapsing activity similar to the one shown for collapsin (Fan and Raper, 1995).

Many glomeruli still form within the necklace area in *Nrp2* and *Sema3f* mutant mice. It is not clear whether the same GC-D$^+$ glomeruli are affected in *Nrp2* and *Sema3f* mutant mice. Moreover, it is not known whether a single GC-D$^+$ neuron sends a single unbranched axon to one glomerulus in wild-type and mutant mice, or whether it has projections to several glomeruli. Some cells in the septal organ also express GC-D, and they may behave differently

than GC-D$^+$ neurons of the MOE in the absence of Nrp2 or Sema3f. Neurons from the Grueneberg ganglion project axons to the necklace area but do not express GC-D, yet they are Nrp2$^+$ (Fuss et al., 2005). These axons are unlikely to contribute to the GC-D$^+$ necklace glomeruli, but could be affected in Nrp2- or Sema3f-deficient mice.

Further studies will address the in vitro effects of Sema3f on GC-D$^+$ axons. It will also be interesting to cross the NP2-Δ and ΔF mutations, to determine if the phenotype of the double mutants is the same as that of the single mutants.

Different classes of V1r-expressing vomeronasal sensory neurons

Our *Sema3f* knockout phenocopies our *Nrp2* knockout for both necklace and vomeronasal glomeruli, whereas mutants in *Sema3b* and *Sema3c* do not show obvious changes. Comparing our findings with a previous study investigating the role of Sema3f in the innervation of apical VSNs to the aAOB (Cloutier et al., 2004), there are some discrepancies. Whereas Cloutier et al. also reported the defasciculation of VSN axons along the medial surface in *Nrp2* or *Sema3f* mutant backgrounds, they could see misplaced axonal growth and glomerular formation within the pAOB only in *Nrp2* mutants but not in *Sema3f* mutants (Cloutier et al., 2004). Moreover, the misplaced glomerular innervation of VSN axons into the MOB (Cloutier et al., 2004) was not detected by us.

One explanation is a difference in the nature of the targeted mutation in *Sema3f*: the mutation used by Cloutier et al. (Cloutier et al., 2004) removes exon 1 and 4 kb of presumptive promoter sequence, whereas our *Sema3f* mutation removes exons 2–15, or 85% of the ORF. Another, more interesting, explanation may lie in the vomeronasal receptor type 1 gene (*V1r*) that is expressed by the VSNs studied: *V1rb2* in our case, and *V1ra1* in the case of Cloutier et al. (Cloutier et al., 2004). There may be heterogeneity among populations of VSNs that express a given V1r from the repertoire of >100 *V1r* genes in mouse (Zhang et al., 2007). V1ra1$^+$ VSNs may respond to other Nrp2 ligands such as Sema3b or Sema3c instead of Sema3f. Since neuropilins need other partners to transduce ligand binding, such as plexins (Tamagnone et al., 2001), cell adhesion molecules (Castellani et al., 2000; Julien et al., 2005), MICALs (Terman et al., 2002) or NIP (Cai and Reed, 1999), V1ra1$^+$ VSNs could express a different receptor complex than V1rb2$^+$ VSNs and respond differently to various semaphorin ligands. The misprojections of V1ra1$^+$ but not V1rb2$^+$ axons into the MOB could be explained by such molecular differences. It is less clear why V1ra1$^+$ axons do not misroute into the pAOB of *Sema3f* mutant mice. Other explanations involve untested members of the class III semaphorin family, such as Sema3e (Miyazaki et al., 1999), or the unknown negative regulation of one class III semaphorin on the action of another to render it an attractant, as is the case for Sema3b or Sema3c acting to reverse the repulsive action of Sema3a on Nrp1-expressing growth cones (Takahashi et al., 1998).

Other semaphorins

A role for Sema3b and Sema3c cannot be ruled out completely. In the case of the anterior commissure (AC), Sema3f first appeared to be the sole ligand responsible for the absence of an AC in *Nrp2* mutant mice (Sahay et al., 2003). In a later study, however, it became clear that Sema3b has a somewhat overlapping yet mostly complementary role in establishing the positioning of the AC as well as causing the attraction or repulsion of various axonal tracts contributing to the AC; the loss of Sema3b induced the defasciculation of parts of the AC (Julien et al., 2005). By contrast, no real function has been established for Sema3c in the nervous system. Some studies suggest that Sema3c can influence hippocampal (Steup et al., 1999), cortical (Gonthier et al., 2006) and cerebellar (Moreno-Flores et al., 2003) neurites in vitro but no investigations in vivo have been reported. Also, the expression of the various plexins can profoundly affect the ability of any member of class III semaphorins to act as either an attractant or repellant (Yaron et al., 2005). Thus a change in the plexin expressed in either *Nrp2* or semaphorin mutant background may have occurred and consequently altered axon behavior.

The authors thank Julie Miwa, Stefan Fuss, and Takeshi Imai for reading the manuscript and useful discussions. P.M. thanks Melissa Berry from The Jackson Laboratory for advice on nomenclature. Supported by NIDCD grants to A.W. and P.M.

References

Axel, R. (2005). Scents and sensibility: a molecular logic of olfactory perception. *Angew. Chem. Int. Ed. Engl.* **38**, 6110-6127.

Belluscio, L., Koentges, G., Axel, R. and Dulac, C. (1999). A map of pheromone receptor activation in the mammalian brain. *Cell* **97**, 209-220.

Bozza, T., Feinstein, P., Zheng, C. and Mombaerts, P. (2002). Odorant receptor expression defines functional units in the mouse olfactory system. *J. Neurosci.* **22**, 3033-3043.

Buck, L. B. (2005). Unraveling the sense of smell. *Angew. Chem. Int. Ed. Engl.* **38**, 6128-6140.

Cai, H. and Reed, R. R. (1999). Cloning and characterization of neuropilin-1-interacting protein: a PSD-95/Dlg/ZO-1 domain-containing protein that interacts with the cytoplasmic domain of neuropilin-1. *J. Neurosci.* **19**, 6519-6527.

Castellani, V., Chedotal, A., Schachner, M., Faivre-Sarrailh, C. and Rougon, G. (2000). Analysis of the L1-deficient mouse phenotype reveals cross-talk between Sema3A and L1 signaling pathways in axonal guidance. *Neuron* **27**, 237-249.

Chen, H., Chedotal, A., He, Z., Goodman, C. S. and Tessier-Lavigne, M. (1997). Neuropilin-2, a novel member of the neuropilin family, is a high affinity receptor for the semaphorins Sema E and Sema IV but not Sema III. *Neuron* **19**, 547-559.

Cloutier, J. F., Giger, R. J., Koentges, G., Dulac, C., Kolodkin, A. L. and Ginty, D. D. (2002). Neuropilin-2 mediates axonal fasciculation, zonal segregation, but not axonal convergence, of primary accessory olfactory neurons. *Neuron* **33**, 877-892.

Cloutier, J. F., Sahay, A., Chang, E. C., Tessier-Lavigne, M., Dulac, C., Kolodkin, A. L. and Ginty, D. D. (2004). Differential requirements for semaphorin 3F and Slit-1 in axonal targeting, fasciculation, and segregation of olfactory sensory neuron projections. *J. Neurosci.* **24**, 9087-9096.

Fan, J. and Raper, J. A. (1995). Localized collapsing cues can steer growth cones without inducing their full collapse. *Neuron* **14**, 263-274.

Feiner, L., Webber, A. L., Brown, C. B., Lu, M. M., Jia, L., Feinstein, P., Mombaerts, P., Epstein, J. A. and Raper, J. A. (2001). Targeted disruption of semaphorin 3C leads to persistent truncus arteriosus and aortic arch interruption. *Development* **128**, 3061-3070.

Feinstein, P. and Mombaerts, P. (2004). A contextual model for axonal sorting into glomeruli in the mouse olfactory system. *Cell* **117**, 817-831.

Fleischer, J., Schwarzenbacher, K., Besser, S., Hass, N. and Breer, H. (2006). Olfactory receptors and signaling elements in the Grueneberg ganglion. *J. Neurochem.* **98**, 543-554.

Fülle, H. J., Vassar, R., Foster, D. C., Yang, R. B., Axel, R. and Garbers, D. L. (1995). A receptor guanylate cyclase expressed specifically in olfactory sensory neurons. *Proc. Natl. Acad. Sci. USA* **92**, 3571-3575.

Fuss, S. H., Omura, M. and Mombaerts, P. (2005). The Grueneberg ganglion of the mouse projects axons to glomeruli in the olfactory bulb. *Eur. J. Neurosci.* **22**, 2649-2654.

Gonthier, B., Nasarre, C., Roth, L., Perraut, M., Thomasset, N., Roussel, G., Aunis, D. and Bagnard, D. (2007). Functional interaction between matrix metalloproteinase-3 and semaphorin-3C during cortical axonal growth and guidance. *Cereb. Cortex* **17**, 1712-1721.

Greer, C. A., Stewart, W. B., Teicher, M. H. and Shepherd, G. M. (1982). Functional development of the olfactory bulb and a unique glomerular complex in the neonatal rat. *J. Neurosci.* **2**, 1744-1759.

Grosmaitre, X., Santarelli, L. C., Tan, J., Luo, M. and Ma, M. (2007). Dual functions of mammalian olfactory sensory neurons as odor detectors and mechanical sensors. *Nat. Neurosci.* **10**, 348-354.

Grueneberg, H. (1973). A ganglion probably belonging to the N. terminalis system in the nasal mucosa of the mouse. *Z. Anat. Entwicklungsgesch.* **140**, 39-52.

Hu, J., Zhong, C., Ding, C., Chi, Q., Walz, A., Mombaerts, P., Matsunami, H.

and Luo, M. (2007). Detection of near-atmospheric concentrations of CO2 by an olfactory subsystem in the mouse. *Science* **317**, 953-957.
Juilfs, D. M., Fülle, H. J., Zhao, A. Z., Houslay, M. D., Garbers, D. L. and Beavo, J. A. (1997). A subset of olfactory neurons that selectively express cGMP-stimulated phosphodiesterase (PDE2) and guanylate cyclase-D define a unique olfactory signal transduction pathway. *Proc. Natl. Acad. Sci. USA* **94**, 3388-3395.
Julien, F., Bechara, A., Fiore, R., Nawabi, H., Zhou, H., Hoyo-Becerra, C., Bozon, M., Rougon, G., Grumet, M., Püschel, A. W. et al. (2005). Dual functional activity of semaphorin 3B is required for positioning the anterior commissure. *Neuron* **48**, 63-75.
Kolodkin, A. L., Levengood, D. V., Rowe, E. G., Tai, Y. T., Giger, R. J. and Ginty, D. D. (1997). Neuropilin is a semaphorin III receptor. *Cell* **90**, 753-762.
Koos, D. S. and Fraser, S. E. (2005). The Grueneberg ganglion projects to the olfactory bulb. *Neuroreport* **16**, 1929-1932.
Kuhn, M. (2003). Structure, regulation, and function of mammalian membrane guanylate cyclase receptors, with a focus on guanylate cyclase-A. *Circ. Res.* **93**, 700-709.
Le Jeune, H. and Jourdan, F. (1991). Postnatal development of cholinergic markers in the rat olfactory bulb: a histochemical and immunocytochemical study. *J. Comp. Neurol.* **314**, 383-395.
Le Jeune, H. and Jourdan, F. (1993). Cholinergic innervation of olfactory glomeruli in the rat: an ultrastructural immunocytochemical study. *J. Comp. Neurol.* **336**, 279-292.
Liberles, S. D. and Buck, L. B. (2006). A second class of chemosensory receptors in the olfactory epithelium. *Nature* **442**, 645-650.
Ma, M., Grosmaitre, X., Iwema, C. L., Baker, H., Greer, C. A. and Shepherd, G. M. (2003). Olfactory signal transduction in the mouse septal organ. *J. Neurosci.* **23**, 317-324.
Meyer, M. R., Angele, A., Kremmer, E., Kaupp, U. B. and Muller, F. (2000). A cGMP-signaling pathway in a subset of olfactory sensory neurons. *Proc. Natl. Acad. Sci. USA* **97**, 10595-10600.
Miyazaki, N., Furuyama, T., Sakai, T., Fujioka, S., Mori, T., Ohoka, Y., Takeda, N., Kubo, T. and Inagaki, S. (1999). Developmental localization of semaphorin H messenger RNA acting as a collapsing factor on sensory axons in the mouse brain. *Neuroscience* **93**, 401-408.
Mombaerts, P. (2004). Genes and ligands for odorant, vomeronasal and taste receptors. *Nat. Rev. Neurosci.* **5**, 263-278.
Mombaerts, P. (2006). Axonal wiring in the mouse olfactory system. *Annu. Rev. Cell Dev. Biol.* **22**, 713-737.
Mombaerts, P., Wang, F., Dulac, C., Chao, S. K., Nemes, A., Mendelsohn, M., Edmondson, J. and Axel, R. (1996). Visualizing an olfactory sensory map. *Cell* **87**, 675-686.
Moon, C., Jaberi, P., Otto-Bruc, A., Baehr, W., Palczewski, K. and Ronnett, G. V. (1998). Calcium-sensitive particulate guanylate cyclase as a modulator of cAMP in olfactory receptor neurons. *J. Neurosci.* **18**, 3195-3205.
Moreno-Flores, M. T., Martin-Aparicio, E., Martin-Bermejo, M. J., Agudo, M., McMahon, S., Avila, J., Diaz-Nido, J. and Wandosell, F. (2003). Semaphorin 3C preserves survival and induces neuritogenesis of cerebellar granule neurons in culture. *J. Neurochem.* **87**, 879-890.
Ring, G., Mezza, R. C. and Schwob, J. E. (1997). Immunohistochemical identification of discrete subsets of rat olfactory neurons and the glomeruli that they innervate. *J. Comp. Neurol.* **388**, 415-434.
Risser, J. M. and Slotnick, B. M. (1987). Suckling behavior in rat pups with lesions which destroy the modified glomerular complex. *Brain Res. Bull.* **19**, 275-281.
Rodolfo-Masera, T. (1943). Su l'esistenza di un particolare organo olfacttivo nel setto nasale della cavia e di altri roditori. *Arch. Ital. Anat. Embryol.* **48**, 157-212.
Rodriguez, I., Feinstein, P. and Mombaerts, P. (1999). Variable patterns of axonal projections of sensory neurons in the mouse vomeronasal system. *Cell* **97**, 199-208.
Roppolo, D., Ribaud, V., Jungo, V. P., Luscher, C. and Rodriguez, I. (2006). Projection of the Grueneberg ganglion to the mouse olfactory bulb. *Eur. J. Neurosci.* **23**, 2887-2894.
Sahay, A., Molliver, M. E., Ginty, D. D. and Kolodkin, A. L. (2003). Semaphorin 3F is critical for development of limbic system circuitry and is required in neurons for selective CNS axon guidance events. *J. Neurosci.* **23**, 6671-6680.
Shinoda, K., Shiotani, Y. and Osawa, Y. (1989). "Necklace olfactory glomeruli" form unique components of the rat primary olfactory system. *J. Comp. Neurol.* **284**, 362-373.
Shinoda, K., Ohtsuki, T., Nagano, M. and Okumura, T. (1993). A possible functional necklace formed by placental antigen X-P2-immunoreactive and intensely acetylcholinesterase-reactive (PAX/IAE) glomerular complexes in the rat olfactory bulb. *Brain Res.* **618**, 160-166.
Steup, A., Ninnemann, O., Savaskan, N. E., Nitsch, R., Püschel, A. W. and Skutella, T. (1999). Semaphorin D acts as a repulsive factor for entorhinal and hippocampal neurons. *Eur. J. Neurosci.* **11**, 729-734.
Takahashi, T., Nakamura, F., Jin, Z., Kalb, R. G. and Strittmatter, S. M. (1998). Semaphorins A and E act as antagonists of neuropilin-1 and agonists of neuropilin-2 receptors. *Nat. Neurosci.* **1**, 487-493.
Tamagnone, L., Artigiani, S., Chen, H., He, Z., Ming, G. I., Song, H., Chedotal, A., Winberg, M. L., Goodman, C. S., Poo, M. et al. (2001). Plexins are a large family of receptors for transmembrane, secreted, and GPI-anchored semaphorins in vertebrates. *Cell* **99**, 71-80.
Terman, J. R., Mao, T., Pasterkamp, R. J., Yu, H. H. and Kolodkin, A. L. (2002). MICALs, a family of conserved flavoprotein oxidoreductases, function in plexin-mediated axonal repulsion. *Cell* **109**, 887-900.
Tian, H. and Ma, M. (2004). Molecular organization of the olfactory septal organ. *J. Neurosci.* **24**, 8383-8390.
Walz, A., Rodriguez, I. and Mombaerts, P. (2002). Aberrant sensory innervation of the olfactory bulb in neuropilin-2 mutant mice. *J. Neurosci.* **22**, 4025-4035.
Walz, A., Omura, M. and Mombaerts, P. (2006). Development and topography of the lateral olfactory tract in the mouse: imaging by genetically encoded and injected fluorescent markers. *J. Neurobiol.* **66**, 835-846.
Weruaga, E., Brinon, J. G., Porteros, A., Arevalo, R., Aijon, J. and Alonso, J. R. (2001). A sexually dimorphic group of atypical glomeruli in the mouse olfactory bulb. *Chem. Senses* **26**, 7-15.
Yang, R. B., Fülle, H. J. and Garbers, D. L. (1996). Chromosomal localization and genomic organization of genes encoding guanylate cyclase receptors expressed in olfactory sensory neurons and retina. *Genomics* **31**, 367-372.
Yaron, A., Huang, P. H., Cheng, H. J. and Tessier-Lavigne, M. (2005). Differential requirement for Plexin-A3 and -A4 in mediating responses of sensory and sympathetic neurons to distinct class 3 Semaphorins. *Neuron* **45**, 513-523.
Zhang, X., Zhang, Z. and Firestein, S. (2007). Comparative genomics of odorant and pheromone receptor genes in rodents. *Genomics* **89**, 441-450.
Zheng, L. M., Ravel, N. and Jourdan, F. (1987). Topography of centrifugal acetylcholinesterase-positive fibres in the olfactory bulb of the rat: evidence for original projections in atypical glomeruli. *Neuroscience* **23**, 1083-1093.